Contents lists available at SCCE

Journal of Soft Computing in Civil Engineering

Journal homepage: www.jsoftcivil.com

Prediction of the Horizontal Displacement of Mechanically Stabilized Earth Wall using Soft Computing

Saloua Hamza [1]; Brahim Lafifi [2,*]; Mohamed Nemissi [3]; Abdelkrim Moussaoui [4]; Ammar Rouaiguia [2]

1. Ph.D. Candidate, Laboratory of Civil Engineering and Hydraulics, 8 may 1945 Guelma University, Guelma, Algeria
2. Professor, Laboratory of Civil Engineering and Hydraulics, 8 may 1945 Guelma University, Guelma, Algeria
3. Professor, Laboratory LabSTIC, 8 may 1945 Guelma University, Guelma, Algeria
4. Professor, Department of Electrical and Automatic Engineering Laboratory (LGEG), 8 may 1945 Guelma University, Guelma, Algeria

* Corresponding author: *blafifi@gmx.fr*

https://doi.org/10.22115/scce.2025.1959

ARTICLE INFO

Article history:
Received: 05 October 2024
Revised: 17 January 2025
Accepted: 02 September 2025

Keywords:
Mechanically stabilized;
Earth (MSE) wall;
Horizontal displacement;
Plaxis;
Prediction;
Machine learning.

ABSTRACT

Mechanically Stabilized Earth (MSE) walls are a construction method that incorporates artificial reinforcement elements like geosynthetics within the soil. This geotechnical engineering technique is favored for reinforced soil structures due to its cost-effectiveness and ease of implementation. The primary goal of this study was to predict the horizontal displacement (U_x) of MSE walls by evaluating the performance of five AI-based machine learning models: multilayer perceptron (MLP), support vector machine (SVM), k-nearest neighbor (KNN), lazy k-star (LKS), and random forest (RF). A dataset of 712 numerical models was created using the finite element software Plaxis 2D and was randomly divided into a 70% training set and a 30% testing set. Each sample contained eight input variables: reinforcement length (L), the vertical spacing of reinforcement (S_v), wall height (H), length of the embankment (B), angle of inclination of the embankment (α), stiffness of reinforcement (EA), friction angle (φ) of the embankment, and unit weight (γ), along with one output response, the horizontal displacement (U_x). The accuracy of the models was assessed using ten statistical metrics. The findings indicated that the MLP model performed the best with a higher coefficient of determination of 0.9498 and a lower mean absolute error of 0.0136, while the SVM model performed the worst (R^2=0.7067, MAE=0.0438). Sensitivity analysis for the MLP model evaluated the relationships between the input parameters and the output response, revealing that wall height (H) had the highest correlation with U_x. In contrast, the stiffness of reinforcement (EA) showed relatively lower correlations with U_x.

How to cite this article: Hamza S, Lafifi B, Nemmissi M, Moussoaui A, Rouaiguia A. Prediction of the horizontal displacement of mechanically stabilized earth wall using soft computing. Journal of Soft Computing in Civil Engineering. 2026;10(3):1959. https://doi.org/10.22115/scce.2025.1959

1. Introduction

Geosynthetic-reinforced soil walls, a widely used type of reinforced earth structure, are commonly employed in transportation infrastructure projects such as highway ramps and bridge approaches. The design, analysis, and monitoring of these structures must follow specific guidelines and principles, which are based on thorough investigations into the behavior of reinforced soils under varying geometric conditions [1].

It is widely acknowledged that these walls integrate artificial reinforcing elements within the soil. Typically, such wall systems employ horizontal layers of geogrids for reinforcement. The primary advantages of mechanically stabilized earth (MSE) wall construction include ease of installation and rapid project completion [2]. Unlike conventional construction methods, these walls do not require formwork or curing. Each reinforcement layer is structurally stable upon placement, eliminating the need for support structures, scaffolding, or cranes [3]. Moreover, MSE walls eliminate the need for extensive exterior facing work, further simplifying and accelerating the construction process [4]. Reinforced soil is extensively used in geotechnical engineering due to its cost-effectiveness, ease of construction, reinforcement advantages, and aesthetic versatility [5].

Soils used for backfill that do not meet the select fill criteria are classified as marginal fill. However, due to the limited availability of select fill materials locally, along with transportation costs and time constraints, locally available marginal soils are often utilized as reinforced and retained backfill [6]. Studies show that backfill can account for approximately 50% to 75% of the total project cost [7]. As a result, substantial cost savings (20–30%) can be achieved by using in-situ or locally available soils instead of importing high-quality, well-graded granular materials [8]. In modern construction, the use of geosynthetic-reinforced soil has become increasingly prevalent, particularly for enhancing the sustainability of various projects, including soil foundations. Over the past four decades, extensive research has been conducted to investigate the behavior of shallow reinforced soil foundations under monotonic loads. Abu-Farsakh et al. [9] found that incorporating geosynthetics in paved roads constructed on soft soil significantly improved performance under simulated traffic conditions. The study quantified these benefits, demonstrating that geosynthetics increased the resilient modulus of the base layer by 25% and allowed for a reduction in base thickness by up to one-third.

Lafifi et al. [10] proposed a novel method to optimize the parameters influencing the bearing capacity of a shallow square foundation on geosynthetic-reinforced sandy soil. Laboratory tests, ANOVA, RSM, ANN, and Multi-Objective Genetic Algorithm were employed to model and optimize the bearing capacity while ensuring cost efficiency. Additionally, extensive full-scale studies conducted by Blivet et al. [11] demonstrated that planar geosynthetic reinforcement can significantly reduce the risk of serious accidents caused by localized sinkholes beneath highways and railway embankments. The integration of geosynthetics in road construction also minimizes pavement deformation induced by vehicular traffic, thereby enhancing both the strength and durability of the pavement [12]. Chen et al. (2018) [13] evaluated the performance of full-scale geosynthetic-reinforced flexible pavements using accelerated wheel load testing. Their findings underscore the effectiveness of geosynthetics in improving pavement durability and reducing deformation, particularly in soft subgrade conditions. One of the key advantages of mechanically stabilized earth (MSE) walls is their inherent flexibility. Research conducted in seismically active regions has shown that these structures exhibit superior resistance to seismic forces compared to rigid concrete structures [14].

Due to the critical importance of reinforced soil structures, numerical methods such as finite difference (FD) analysis are extensively utilized for performance-based design, as emphasized in [15]. The inherent

variability in the geomechanical properties of soils necessitates reliability analysis for retaining walls. Recent studies on reinforced retaining walls have incorporated variations in reinforcing material properties [16]. Yu and Bathurst [17] explored the use of Monte Carlo simulation to evaluate the Hasofer–Lind reliability index for engineering design optimization. Their research, along with other studies, has focused on understanding the lateral deformation behavior of reinforced retaining walls. Sekfali and Lafifi [18] conducted a reliability analysis of mechanically reinforced earth walls by integrating uncertainties through random variables and a deterministic model for maximum horizontal displacement. Employing artificial neural networks (ANN) and multi-objective genetic algorithms (MOGA), they optimized the Hasofer-Lind reliability index, emphasizing the impact of parameter distributions and identifying critical uncertainties to ensure a robust and reliable design.

Despite the fact that finite element modeling (FEM) is a powerful tool for addressing intricate geotechnical challenges and delivering precise results [19], one of its primary limitations is its computational intensity. Solving complex geotechnical problems, particularly those involving large-scale structures or fine meshes, often demands significant computational resources and time. For example, simulating the behavior of a mechanically stabilized earth (MSE) wall under varying load conditions can take hours or even days, rendering it impractical for real-time decision-making or iterative design processes [20]. Another limitation of traditional numerical methods is their rigidity and lack of adaptability. Once a numerical model is established, modifying input parameters or adjusting the geometry typically necessitates a complete re-simulation, which is both time-consuming and resource-intensive [21]. This inflexibility hinders the exploration of multiple design scenarios or the incorporation of new data, thereby restricting the overall adaptability of the design process. Additionally, the use of numerical modeling requires specialized software and technical expertise, which can be costly and may not be readily accessible for many engineering projects, especially those with limited budgets or in resource-constrained environments. These barriers often prevent smaller engineering firms or projects with restricted resources from fully utilizing the capabilities of numerical modeling [22].

In contrast, machine learning (ML) techniques, particularly those based on artificial intelligence (AI), offer a promising alternative to traditional numerical modeling. ML models are data-driven, meaning they learn patterns and relationships directly from data without relying on explicit physical laws or assumptions. This enables them to effectively capture complex, nonlinear interactions between input and output variables, which are often challenging to model analytically [23]. Machine learning holds significant potential for addressing a wide range of challenges across various industries. By collecting and analyzing extensive datasets, ML algorithms can accurately predict outcomes and classify data [24]. Additionally, innovative metaheuristic algorithms have been developed to optimize big data analysis, further enhancing the capabilities of ML in solving complex problems [25]. In geotechnical engineering, soft computing methods are increasingly being utilized for predictive applications. For instance, Goudjil and Arabet (2021) [26] developed a neural model to predict the deflection of laterally loaded piles near slopes using a two-part approach. The neural model achieved high accuracy ($R^2 = 0.9647$) with minimal errors, demonstrating its effectiveness. Similarly, Belaabed et al. [27] employed artificial neural networks (ANNs) to predict the relative head of submerged piano key weirs (PK-Weirs) based on experimental data. Their results highlighted the capability of neural networks to enhance the accuracy of hydraulic performance predictions for submerged PK-Weirs. Lafifi et al. [28] focused on optimizing both the bearing capacity and construction cost of strip footings on soft soils reinforced with stone columns by integrating artificial neural networks (ANNs) with multi-objective optimization techniques. Their study utilized ANN models coupled with a genetic algorithm to determine the optimal design variables for the problem. Additionally, Goudjil et al. [29] explored the use of XGBoost and Random Forest ensemble algorithms to predict soil limit pressure,

providing a cost-effective alternative to pressure meter tests (PMTs). Both models demonstrated high accuracy and low RMSE values, confirming their reliability and practical applicability.

The mechanical behavior of geosynthetic-reinforced soil retaining walls is highly complex, necessitating detailed research to analyze stability, deformation patterns, failure mechanisms, and the influence of geometric parameters [30]. Unlike conventional approaches that often rely on simplifying assumptions, artificial intelligence (AI) models are inherently data-driven, enabling them to adapt to and capture intricate data patterns. As a result, machine learning (ML) techniques have gained significant traction in the study of geosynthetic-reinforced soils, offering more precise, efficient, and reliable solutions for understanding and predicting their behavior [31].

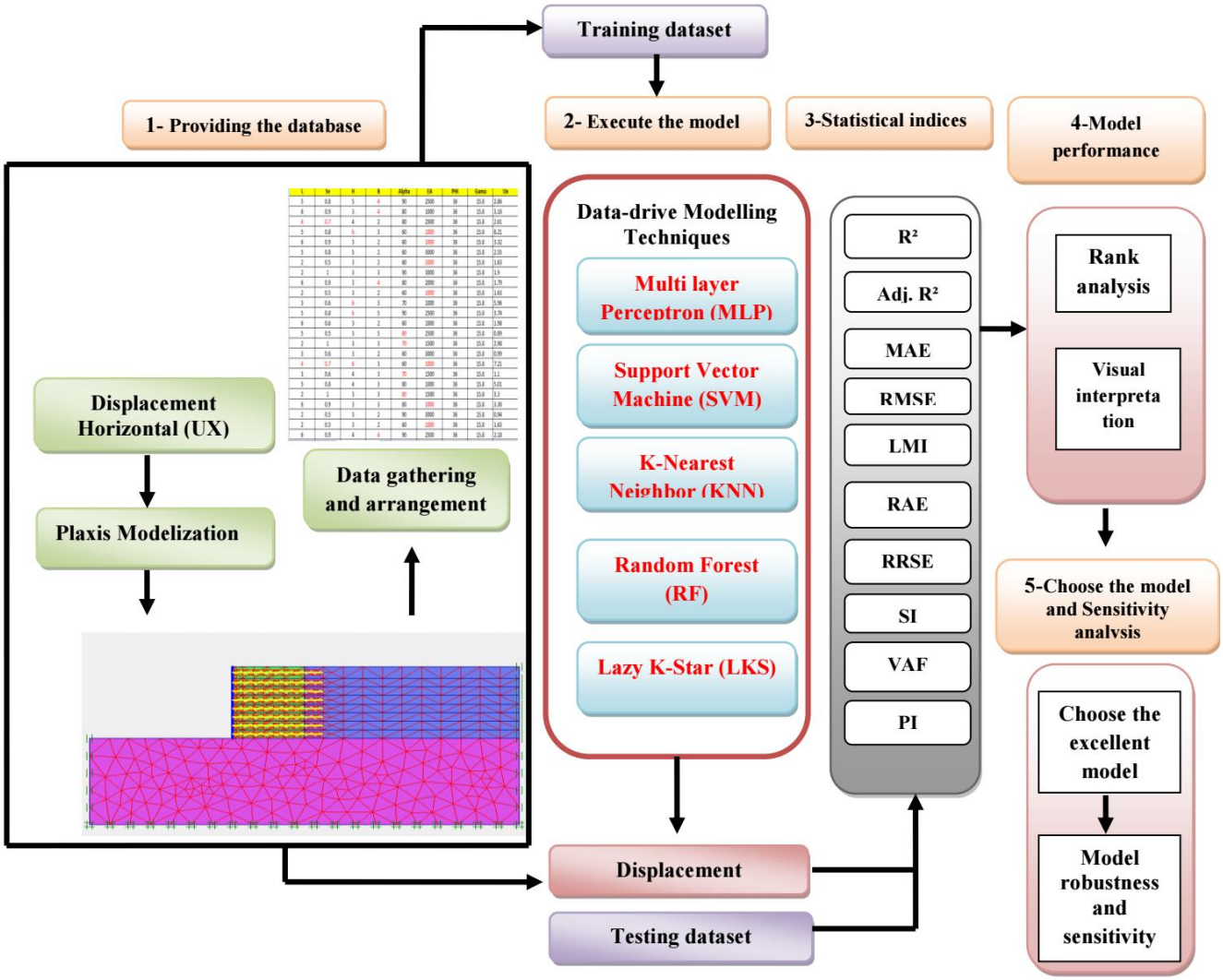

Fig. 1. Research framework used in this study.

For these reasons, this research aims to develop a soft computing model to predict the horizontal displacement of Mechanically Stabilized Earth (MSE) walls reinforced with geogrids, using granular sand as the backfill material. The study utilizes finite element (FE) software PLAXIS 2D to compute horizontal displacements and introduces a novel approach by leveraging machine learning techniques, including Multi-Layer Perceptron (MLP), Support Vector Machine (SVM), Replace with: Lazy K-Star (LKS), K-Nearest Neighbors (KNN), and Random Forest (RF).

The dataset comprises eight input variables: reinforcement length (L), vertical spacing (S_v), wall height (H), embankment length (B), embankment inclination angle (α), reinforcement stiffness (EA), friction angle (φ), and unit weight (γ), with horizontal displacement (U_x) as the output variable. This approach aims to enhance the accuracy and efficiency of predicting MSE wall behavior under varying conditions. To evaluate the performance of the machine learning models, this study employs a comprehensive set of metrics, including Symmetric Mean Absolute Percentage Error (SMAPE), Root Mean Square Error (RMSE), Coefficient of Determination (R^2), Mean Absolute Error (MAE), Scatter Index (SI), Relative Absolute Error (RAE), Root Relative Squared Error (RRSE), Legate and McCabe's Index (LMI), Variance Accounted For (VAF), and Adjusted Coefficient of Determination (Adj. R^2). A thorough ranking analysis is conducted to identify the best-performing soft computing model, supported by visual interpretation tools such as Taylor diagrams, regression error characteristic (REC) curves, and violin plots. Additionally, sensitivity and robustness analyses are performed to further validate the reliability and effectiveness of the adopted machine learning models. Figure 1 illustrates the methodology employed in this research.

2.Material and methods

2.1. Problem definition

Figure 2 illustrates the geometry of the analyzed problem. The model consists of three distinct types of soils. This study focuses on a mechanically stabilized earth (MSE) wall of height H, reinforced with layers of geosynthetic materials. These reinforcement layers are defined by their tensile stiffness (EA), vertical spacing (S_v), and length (L). The backfill used has a length (B) and an inclination angle (α). It was modeled as a homogeneous and isotropic material following the Mohr-Coulomb (MC) elasticity criterion, characterized by unit weight (γ) and internal friction angle (φ).

To simplify the presentation of the calculated results, the lateral displacement of the wall U_x, is expressed as a function of the relevant problem variables. These variables include the height of the wall (H), the width of the selected backfill (B), the length of the reinforcement layers (L), the vertical spacing between these layers (S_v), their tensile stiffness (EA), the inclination angle of the backfill (α), the internal friction angle of the backfill (φ), and its unit weight (γ). This relationship can be expressed as:

$$Ux = f(H, B, L, S_v, EA, \alpha, \varphi, \gamma) \quad (1)$$

The ranges of the variables for the problem addressed are specified in the table 1:

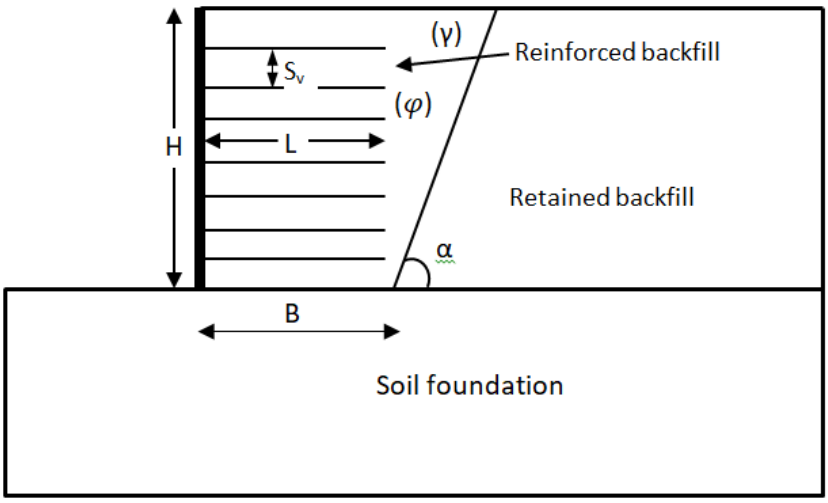

Fig. 2. Geometric of the Mechanically Stabilized Earth (MSE) wall model.

Table 1
Ranges of parameters used in the study.

Item	Attributes (Unit)	Values
Reinforced backfill geometry	Height H(m)	3, 4, 5, 6
	Width B(m)	2, 3, 4, 5
Reinforced backfill properties	Friction angle φ (°)	36, 40, 45,50
	Unit weight γ (KN/m^3)	15.8, 17.1, 18.7, 21.2
Reinforcement Properties	Reinforcement spacing, S_v(m)	0.5, 0.6, 0.7, 0.8, 0.9, 1
	Reinforcement length, L(m)	2, 3, 4, 5, 6
	Reinforcement stiffness (KN/m)	1000, 1500, 2000, 2500, 3000
	Angle of inclination α(°)	60, 70, 80, 90

2.2. Validation of the proposed model

A 6-meter-high reinforced earth wall, composed of four layered panels and eight levels of geosynthetic reinforcement, was simulated using the Plaxis 2D finite element software. The simulation, based on the plane strain condition and the model suggested by Abdelouahab et al. (2011) [32], employed plate elements for the panels and geogrid elements for the four-meter-long reinforcements (see Figure 3).

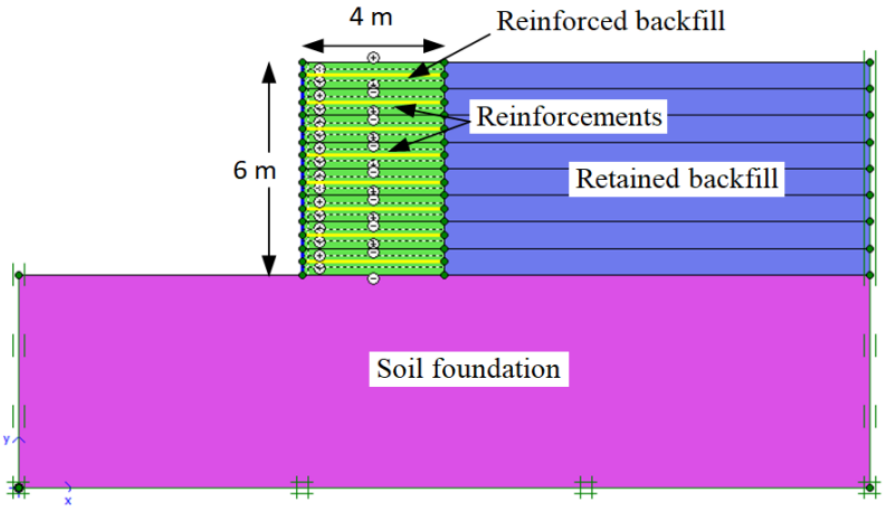

Fig. 3. Geometric of the validation model.

The model's reinforcement properties were determined by averaging the geometric properties across the modeled width. It incorporates three soil types (Figure 3), detailed in Table 2, with the reinforced backfill represented by uniform Hostun RF sand [33]. A linear elastic perfectly plastic Mohr-Coulomb model, calibrated using triaxial test data [32], describes the reinforced and retained embankment's behavior. The foundation soil uses a simpler linear elastic model. Boundary conditions fix both horizontal and vertical displacements at the model's base, and only horizontal displacements at the lateral sides.

A numerical model of a reinforced earth wall employs GeoStrap 50 (GS50) geosynthetic reinforcements, common in such structures. The model accounts for the typical real-world use of paired 50mm wide strips (250mm total width) by using Plaxis's "Geogrid" elements, which consider tension, compression, and shear forces. For greater accuracy, the reinforced backfill placement is simulated in 0.375m layers over three construction phases (Table 2 details material properties).

The wall's construction was simulated in three stages within the Plaxis 2D software. Each stage involved adding a concrete panel, two layers of reinforced backfill, and a layer of reinforcement, allowing the model to reach equilibrium after each addition. This process was repeated until the 6-meter height was achieved.

The analysis assumed drained conditions and neglected the presence of a water table. The interface friction angle was modeled as two-thirds of the soil's friction angle.

Table 2
Geomechanical characteristics of the elements model.

Properties (unity)	Reinforced backfill	Retained backfill	Foundation soil	Concrete panel	reinforcement
Constitutive model	Mohr Coulomb	Mohr Coulomb	Elastic linear	Elastic linear	-
Young modulus E (MPa)	50	30	50	15000	1000
Poisson's ratioυ	0.3	0.3	0.3	0.2	-
Unit weight γ (KN/m3)	15.8	18	20	25	-
Friction angle φ (°)	36	30	-	-	-
Dilatancy angle Ψ (°)	06	0	-	-	-
Cohesion C (KPa)	0	0	-	-	-

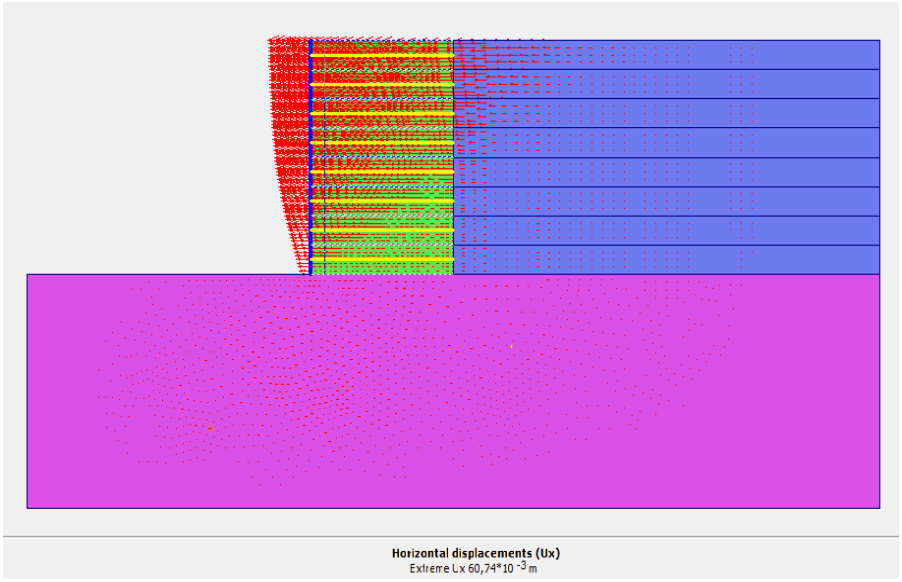

Fig. 4. Horizontal displacements U_x (mm) in the reinforced earth wall with Plaxis 2D.

The results obtained in terms of displacements, horizontal (U_x), vertical (U_y), and total (U)are compared to those of the existing solutions reported byAbdelouahab et al. (2011) [32], as shown in Table 3. The total displacement was calculated using Equation 2.

$$|U|=\sqrt{(U_x{}^2+U_y{}^2)} \tag{2}$$

Table 3 presents the results for the total, horizontal, and vertical displacements. The displacement results from our study align closely with those reported by Abdelouahab et al. (2011) [32], demonstrating consistency and validation of the model. In our study case, the maximum horizontal displacement $U_{xmax}$was taken into account (Fig. 4) in the remainder of the research work.

Table 3
Results in term of displacements.

	$\|U\|$ (mm)	$\|U_x\|$(mm)	$\|U_y\|$(mm)
Abdelouahab et al. 2011	78	61	53
Current study	78.13	60.74	52.52

2.3. Collection and normalization of the data base

A large-scale database of 712 numerical simulations was generated using extensive finite element modeling (FE) through Plaxis 2D software. To ensure consistency in units and prevent overfitting during model development, all input and output parameters were normalized to a range between 0 and 1. This normalization process, described in Equation (3), was adapted from the studies of Ajibona et al. (2022) [34] and Lawal et al. (2021) [35].

$$Y_i = \frac{X_i - X_{min}}{X_{max} - X_{min}} \quad (3)$$

Where X_i, X_{min} and X_{max} present the observed, minimum and maximum values of the data set, respectively.

To ensure consistent and meaningful analysis within the model, input and output parameters are standardized by scaling them to a common range. This normalization process facilitates accurate comparison and analysis of the parameters. Table 4 provides a detailed statistical overview of the dataset. The input parameters include factors such as reinforcement length, spacing, wall height, embankment dimensions, reinforcement stiffness, and soil properties (friction angle and unit weight), all of which have been identified as significant influences on the horizontal displacement (U_x) based on existing research. To maintain data integrity and model reliability, both input parameters and the output response (U_x) are constrained within specific minimum and maximum values, with each parameter having its own defined range.

Table 4
Statistical details of various input and output parameters.

Parameter (Unit)	Min	Max	Mean	SD	Median	Mode	Skewness	Kurtosis	Range
Reinforcement length (L) (m)	2	6	3.888	1.419	4.0	4.0	0.0806	-1.2434	4.0
Vertical spacing of reinforcement (S_v) (m)	0.5	1	0.734	0.185	0.8	0.5	0.011	-1.490	0.5
Height wall (H) (m)	3	6	4.298	1.323	4.0	3.0	0.2734	-1.698	3.0
Length of the embankment (B) (m)	2	5	3.517	0.901	4.0	4.0	-0.558	-0.729	3.0
Angle of inclination of the embankment(α) (°)	60	90	71.57	10.80	70.0	70.0	0.569	-0.945	30.0
Stiffness of reinforcement (EA) (KN/m)	1000	3000	1651.6	789.89	1000	1000	0.625	-1.312	2000
Friction angle (φ) (°)	36	50	42.75	5.266	42.5	36.0	0.1102	-1.396	14
Unit weight (γ) (KN/m^3)	15.8	21.2	18.2	2.015	17.9	15.8	0.367	-1.241	5.399
Horizontal displacement (U_x) (mm)	0.63	11.5	2.401	1.686	1.96	0.69	1.943	5.003	10.92

The correlation analysis presented in Figure 5 reveals that the majority of relationships between input and output variables fall within the "moderate" correlation range. A moderate correlation signifies a balanced influence between input and output variables, indicating a favorable condition for model performance. This level of correlation suggests that the input parameters are sufficiently influential on the output (U_x) without being overly dominant, which is ideal for developing robust and reliable predictive models.

The correlation matrix reveals that the dependent variable, horizontal displacement (U_x), is most strongly influenced by wall height (H) with a correlation coefficient of 0.56, and vertical spacing of reinforcement (S_v) with a coefficient of 0.25, both showing moderate positive correlations, indicating that taller walls and wider reinforcement spacing lead to greater displacement. The angle of inclination (α) exhibits a weak correlation (0.00), suggesting it has no significant effect on displacement, while unit weight (γ) shows a moderate negative correlation (-0.42), indicating that heavier materials reduce displacement. Conversely,

the length of the embankment (B) and reinforcement length (L) show weak correlations (0.01 and **0.07**, respectively), implying they have little effect**,** while friction angle (φ) has a moderate negative correlation (-0.44**)**, suggesting higher soil friction reduces displacement. The stiffness of reinforcement (EA) has a moderate negative correlation (-0.35), indicating it has a moderate impact on reducing U_x. These relationships highlight the key factors controlling horizontal displacement in MSE walls, with wall height and reinforcement spacing being the most influential.

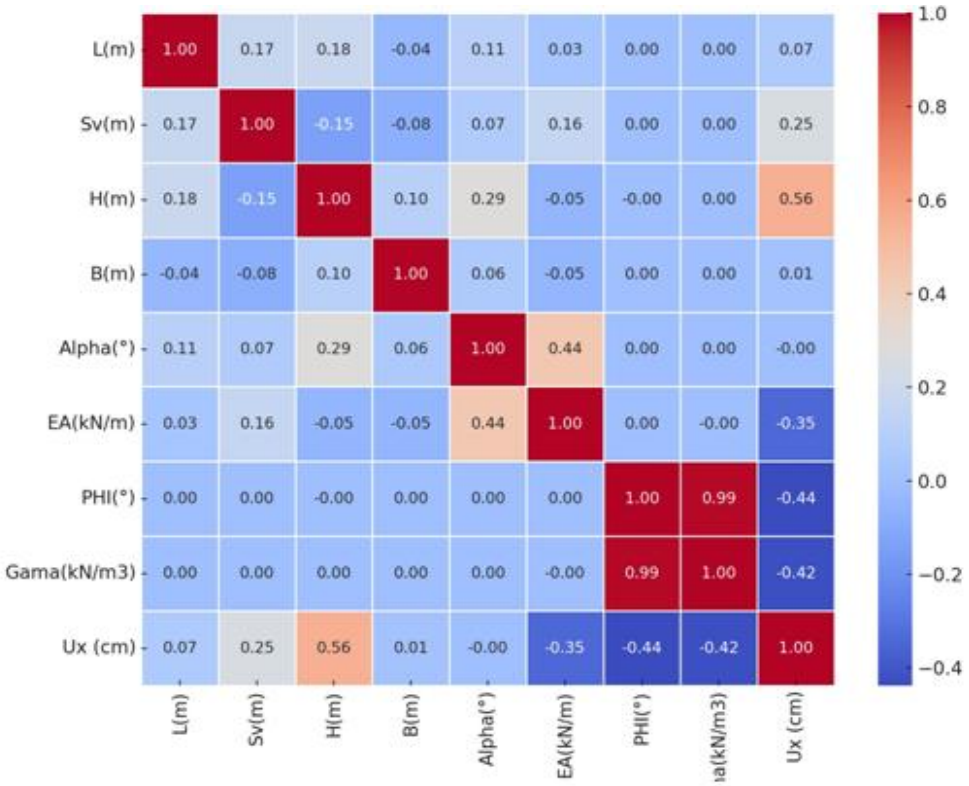

Fig.5. Correlation matrix of the input variables.

3.Theory of methods

This study explores the application of statistical concepts and data-driven machine learning (ML) methods to predict the horizontal displacement of mechanically stabilized earth (MSE) walls. A dataset of 712 randomly selected samples was used to train and test five ML models: multilayer perceptron (MLP), support vector machine (SVM), lazy k-star (LKS), k-nearest neighbors (KNN), and random forest (RF). The research framework includes a database comprising PLAXIS modeling results and corresponding horizontal displacement values. This database was divided into training and testing subsets. In addition to the five ML models, ten statistical indices were evaluated. After implementing and comparing the models, the best-performing model was identified and selected.

3.1. Multilayer perceptron (MLP)

Multilayer Perceptron (MLP) neural networks, inspired by biological neural networks, are a supervised machine learning method used for knowledge acquisition and inference. This process involves two phases: training and prediction. MLP's ability to approximate complex nonlinear relationships between input and output data makes it a powerful tool for machine learning, as demonstrated by various researcher[36,37]. Multi-Layer Perceptron (MLP) neural networks are highly versatile machine learning techniques known for their ability to model complex, nonlinear relationships between input data and output targets. This adaptability has made MLP one of the most widely used methods in machine learning [38,39]. An MLP

network is structured with three interconnected layers: an input layer, a hidden layer, and an output layer. This study uses an input layer with eight nodes, one for each of the eight influencing variables.

The performance of the multilayer perceptron (MLP) is highly sensitive to the number of neurons in its hidden layer. Too few neurons cause underfitting, where the model is too simple to accurately represent the data. Too many neurons lead to overfitting, creating a model that performs well on training data but poorly on unseen data [40].

Hidden layer neurons compute a weighted sum of their inputs from the previous layer, plus a bias term (λ_k). This sum (V_k) is then transformed by a sigmoid activation function, g(.), to generate the neuron's output (The MLP architecture is illustrated in Figure 6).

$$\sum V_k = \lambda_k + \sum_{i=1}^{m} w_{ik} x_i \tag{4}$$

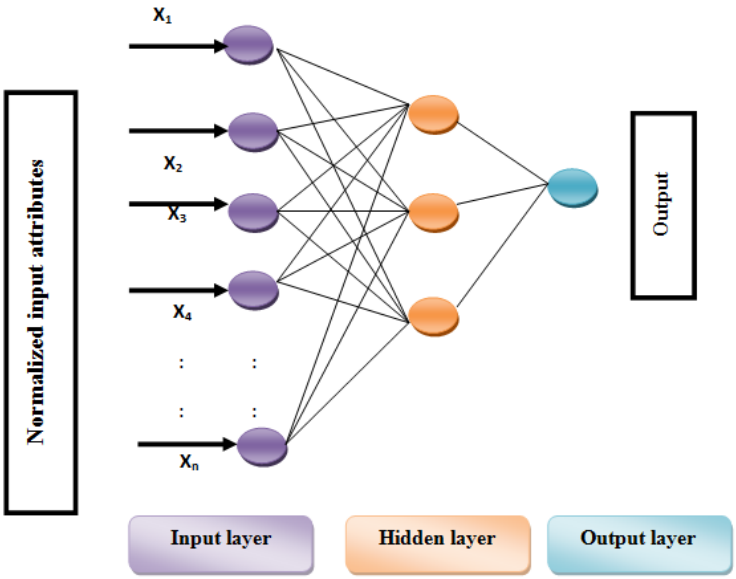

Fig.6. Typical architecture of MLP.

3.2. Support vector machine (SVM)

Support Vector Machine (SVM), developed by Vapnik and Cortes (1995) [41], is a powerful machine learning technique used for both classification and regression. SVM is valued for their accuracy, ability to handle high-dimensional data, robustness, and resistance to noise[42]. Its successful application in various fields, including classification and regression tasks, has been well-documented [43].

SVM is particularly well-suited for small to medium-sized classification problems. It seeks the best hyperplane to divide data points into their different classes within an N-dimensional space. A hyperplane is essentially a plane that divides data linearly, with a line representing a hyperplane in two dimensions and a plane in three dimensions. Equation (5) provides the theoretical foundation for the SVM algorithm.

$$T = \{(x_i, y_i); i = 1,2,3 \dots \dots \dots . . n\} \tag{5}$$

Given a dataset with n-dimensional feature vectors x_i and y_i, where x_i belongs to the set X and y_i takes values of either -1 or +1, a linear relationship between the data can be represented using linear equations (6) and (7).

$$W^T x + b = 0 \tag{6}$$

$$W=\{w_1; w_2; w_3; \dots w_n\} \tag{7}$$

Here, w defines the hyperplane itself, and b represents the hyperplane's distance from the origin. Equation (8) calculates the distance between any point X and this hyperplane [44].

$$\gamma = \frac{|w^T x+b|}{\|w\|} \tag{8}$$

3.3. K-Nearest neighbor (KNN)

K-Nearest Neighbors (KNN), introduced by Altman in 1992 [45], is a supervised machine learning method. It classifies new data points based on their proximity to existing, labeled data points. A new point is assigned to the class most common among its k nearest neighbors (where k is a user-specified value). Distance is calculated using metrics like Euclidean, Manhattan, or Minkowski distance (Equation 9). KNN's performance depends on the choice of k, the distance metric, and the quality of the training data, and it can be used for both classification and regression.

$$\mathrm{d}(x,y)=\sqrt{\sum_{i=1}^{n}(x_i-y_i)^2} \tag{9}$$

3.4. Random forest (RF)

Random Forest (RF), developed by Ho in 1995 [46], is an ensemble learning method used for classification and regression. It builds numerous decision trees and averages their predictions, creating a "forest" that reduces overfitting thanks to bootstrap aggregating. This ensemble approach leads to more robust and stable results [47]. Users can customize the Random Forest model by adjusting parameters such as the number of trees, nodes, and variables. While more trees generally improve accuracy, it increases computational cost. However, because trees are built independently and use out-of-bag error estimation, overfitting is not a significant concern even with a large number of trees. Breiman 2001 [47] provides a detailed description of the algorithm.

3.5. Lazy K-Star (LKS)

Lazy learning, unlike eager learning which performs most computations during training, defers the bulk of its processing until a prediction is requested. Lazy k-star (LKS) is a lazy learning algorithm that uses on-demand classification based on the training data.LKS does not infer predictions from specific instances during training. Instead, it stores the entire dataset in memory and generates responses based on the nearest neighbor approach when a query is received. The K-Star algorithm condenses all potential connections between two data points into a single category, providing a concise representation of their relationship [48]. This method calculates the probability of all possible data point transformations to understand their relationships. This entropy-based approach surpasses traditional rule-based methods by better handling missing data and shared attributes. The resulting classification function then predicts the class of new data points. For instance, a new test data point A would be categorized based on the most frequent class among its k nearest neighbors, B_i. Equation (10) represents the LKS formulation [49].

$$K^*(B_i, A_i) = -\log P^*(B_i, A_i) \tag{10}$$

In this context, P* represents the probability function, which calculates the probability of all possible paths leading from instance A to instance B.

4. Model performance based on statistical indices

The study evaluates model performance using ten statistical indicators, divided into goodness of fit and prediction error metrics. Goodness of fit metrics, such as R^2, Adjusted R^2, Variance Accounted For (VAF),

Legate and McCabe's Index (LMI), and Predictive Index (PI), measure how well the model's predictions align with observed data, with higher values indicating better performance. Prediction error metrics, including Root Mean Square Error (RMSE), Mean Absolute Error (MAE), Scatter Index (SI), Relative Absolute Error (RAE), and Root Relative Squared Error (RRSE), quantify the deviation between predicted and observed values, with lower values indicating greater accuracy. The mathematical formulas for all the indices, including RMSE, R^2, MAE, SI, RAE, RRSE, PI, LMI, VAF, and Adj.R^2, are provided in equations (11-20).

$$RMSE = \sqrt{\frac{1}{n}\sum_{i=1}^{n}(X_i - Y_i)^2} \tag{11}$$

$$R^2 = 1 - \frac{\sum_{i=1}^{n}(X_i - Y_i)^2}{\sum_{i=1}^{n}(X_i - \overline{X})^2} \tag{12}$$

$$MAE = \frac{1}{n}\sum_{i=1}^{n}|X_i - Y_i| \tag{13}$$

$$SI = \frac{RMSE}{\overline{X}} \tag{14}$$

$$RAE = \frac{\sum_{i=1}^{n}|X_i - Y_i|}{\sum_{i=1}^{n}|X_i - \overline{X}|} \tag{15}$$

$$RRSE = \sqrt{\frac{\sum_{i=1}^{n}(X_i - Y_i)^2}{\sum_{i=1}^{n}(X_i - \overline{X})^2}} \tag{16}$$

$$PI = adj.R^2 + (0.01xVAF) - RSME \tag{17}$$

$$VAF = \left(1 - \frac{\sum_{i=1}^{n}(X_i - Y_i)^2}{\sum_{i=1}^{n}(X_i - \overline{X})^2}\right)x100\% \tag{18}$$

$$LMI = 1 - \frac{\sum_{i=1}^{n}|X_i - Y_i|}{\sum_{i=1}^{n}|X_i - \overline{X}|} \tag{19}$$

$$Adj.R^2 = 1 - \left(\frac{(n-1)(1-R^2)}{(n-p-1)}\right) \tag{20}$$

Here, Xi represents the i^{th} observed value, Yi represents the i^{th} predicted value, $\overline{X}$ represents the mean value of observed values, $\overline{Y}$ represents the mean value of predicted values, n represents the total number of data samples, and p represents the number of input parameters.

5. Results and discussion

5.1. Model performance and comparison

5.1.1. Rank analysis

This research investigates the prediction of horizontal displacement in (MSE) walls using a range of machine-learning methods, including MLP, SVM, KNN, LKS, and RF. The study employed a dataset of 712 samples, which were divided into a 70% training set and a 30% testing set. Table 5 summarizes the key parameters used in each of the developed models.

The performance of a model is assessed using a combination of metrics. High values for R^2, LMI, VAF, PI, and Adjusted R^2 indicate a strong correlation between predicted and observed values, with a perfect match

represented by a value of 1. Conversely, low values for RMSE, MAE, RRSE, RAE, and SI suggest better accuracy. RMSE, RRSE, RAE, SI, and MAE are commonly used to quantify the errors in predictions. MAE represents the average error without considering its direction, while RMSE emphasizes larger errors by squaring them before averaging. Ideally, all these error metrics should be 0 for a perfect model. SI, the ratio of RMSE to the average observed value, provides a relative measure of accuracy, with lower values indicating better performance.

Table 5
Main parameters of the models.

Name	Parameter
MLP	Hidden layers = 20; Learning rate = 0.3; momentum = 0.2
SVM	Complexity parameter C=5.0 ; kernel = polykarnel ; num decimal places = 1
KNN	KNN =2; nearest Neighbour Search Algorithm = Linear NN Search
L KS	Global bland=20
RF	No; num iteration =100; max depth = 4

The Multi-Layer Perceptron (MLP) model consistently demonstrated superior performance, achieving the highest R^2 values (0.9818 in training and 0.9498 in testing), which indicates a very strong correlation between predicted and observed values. Additionally, it had the lowest error metrics, with MAE values of 0.0124 in training and 0.0136 in testing, and RMSE values of 0.0214 in training and 0.0319 in testing, signifying high accuracy and minimal prediction error.

Table 6
Performance of all the machine learning models in training dataset.

Model	Statistical indices									
	R^2	Adj. R^2	MAE	RMSE	LMI	RAE	RRSE	SI	VAF	PI
MLP	0.9818	0.9817	0,0124	0.0214	0.9818	0.1091	0.1350	0.1304	0.9819	0.9702
SVM	0.7348	0.7342	0.0457	0.0819	0.7348	0.3998	0.5150	0.4988	0.7512	0.6599
KNN	0.9569	0.9568	0.0111	0.0330	0.9569	0.0955	0.2077	0.1973	0.9569	0.9334
LKS	0.8710	0.8707	0.0383	0.0571	0.8710	0.3356	0.3592	0.3479	0.8710	0.8223
RF	0.9588	0.9588	0.0130	0.0322	0.9588	0.1139	0.2029	0.1965	0.9589	0.9361

The Random Forest (RF) model followed closely, with R^2 values of 0.9588 in training and 0.9004 in testing, and competitive error metrics (MAE of 0.0130 in training and 0.0251 in testing, RMSE of 0.0322 in training and 0.0481 in testing), making it a strong and reliable alternative for predictive tasks. The K-Nearest Neighbors (KNN) model also performed well, with R^2 values of 0.9569 in training and 0.8618 in testing, though its error metrics were slightly higher (MAE of 0.0111 in training and 0.0306 in testing, RMSE of 0.0330 in training and 0.0567 in testing). Conversely, the Lazy K-Star and Support Vector Machine (SVM) models exhibited comparatively weaker predictive capabilities. LKS achieved moderate R^2 values (0.8710 in training and 0.7988 in testing) and higher error metrics (MAE of 0.0383 in training and 0.0444 in testing, RMSE of 0.0571 in training and 0.0684 in testing). SVM had the lowest performance across both datasets, with R^2 values of 0.7348 in training and 0.7067 in testing, and the highest error metrics (MAE of 0.0457 in training and 0.0438 in testing, RMSE of 0.0819 in training and 0.0826 in testing), indicating significant difficulties in accurately generalizing predictions from the training data to the testing data.

Scores were assigned based on various statistical performance indicators (detailed in Tables 6, 7, and 8) and summed to obtain a total ranking score for each model. The MLP model achieved the highest total ranking score of 99, indicating it outperformed all other models. RF and KNN models followed closely with scores of 79 and 62, respectively. In contrast, LKS and SVM models obtained significantly lower

scores of 39 and 20, suggesting they performed less well than the top-performing MLP, RF, and KNN models across all evaluated metrics.

Table 7
Performance of all the machine learning models in testing dataset.

Model	Statistical indices									
	R^2	Adj. R^2	MAE	RMSE	LMI	RAE	RRSE	SI	VAF	PI
MLP	0.9498	0.9495	0.0136	0.0319	0.9498	0.1324	0.2224	0.2120	0.9498	0.9271
SVM	0.7067	0.7053	0.0438	0.0826	0.7067	0.4017	0.5416	0.4970	0.7115	0.6299
KNN	0.8618	0.8612	0.0306	0.0567	0.8618	0.2809	0.3717	0.3412	0.8624	0.8131
LKS	0.7988	0.7978	0.0444	0.0684	0.7988	0.4074	0.4486	0.4117	0.7988	0.7374
RF	0.9004	0.8999	0.0251	0.0481	0.9004	0.2302	0.3156	0.2896	0.9005	0.8608

Table 8
Detail of the rank analysis.

Model	MLP		SVM		KNN		LKS		RF	
	TR	TS	TR	TS	TR	TS	TR	TS	TR	TS
R^2	5	5	1	1	3	3	2	2	4	4
Adj. R^2	5	5	1	1	3	3	2	2	4	4
MAE	5	5	1	2	3	3	2	1	4	4
RMSE	5	5	1	1	3	3	2	2	4	4
LMI	5	5	1	1	3	3	2	2	4	4
RAE	4	5	1	1	5	3	2	2	3	4
RRSE	5	5	1	1	3	3	2	2	4	4
SI	5	5	1	1	3	3	2	2	4	4
VAF	5	5	1	1	3	3	2	2	4	4
PI	5	5	1	1	3	3	2	2	4	4
Total	49	50	10	10	32	30	20	19	39	40

The MLP model exhibited the best performance among all models, both in training and testing datasets. RF and KNN models followed closely, ranking second and third, respectively. In contrast, LKS and SVM models showed weaker predictive capabilities compared to the other approaches.

Figure 7 compares the performance of the proposed machine learning models (MLP, RF, KNN, LKS, and SVM) by examining the correlation between their predicted and observed values on both training and testing datasets. The MLP model stands out with the strongest correlation, indicating its ability to effectively learn from the data and generalize well to new examples. The RF model, while demonstrating good correlation, falls short of the MLP's performance. The KNN and LKS models also perform well but exhibit slightly weaker correlations. In contrast, the SVM model shows moderate to weak correlations, suggesting limitations in capturing complex relationships within the data. This finding highlights the importance of carefully selecting and tuning models based on the specific characteristics of the data to achieve optimal predictive accuracy.

Figure 8 visually represents the overall ranking scores for the MLP, SVM, KNN, LKS, and FR models. It clearly shows that the MLP model achieved the highest ranking, outperforming all other computational models in predicting the horizontal displacement of the (MSE) wall.

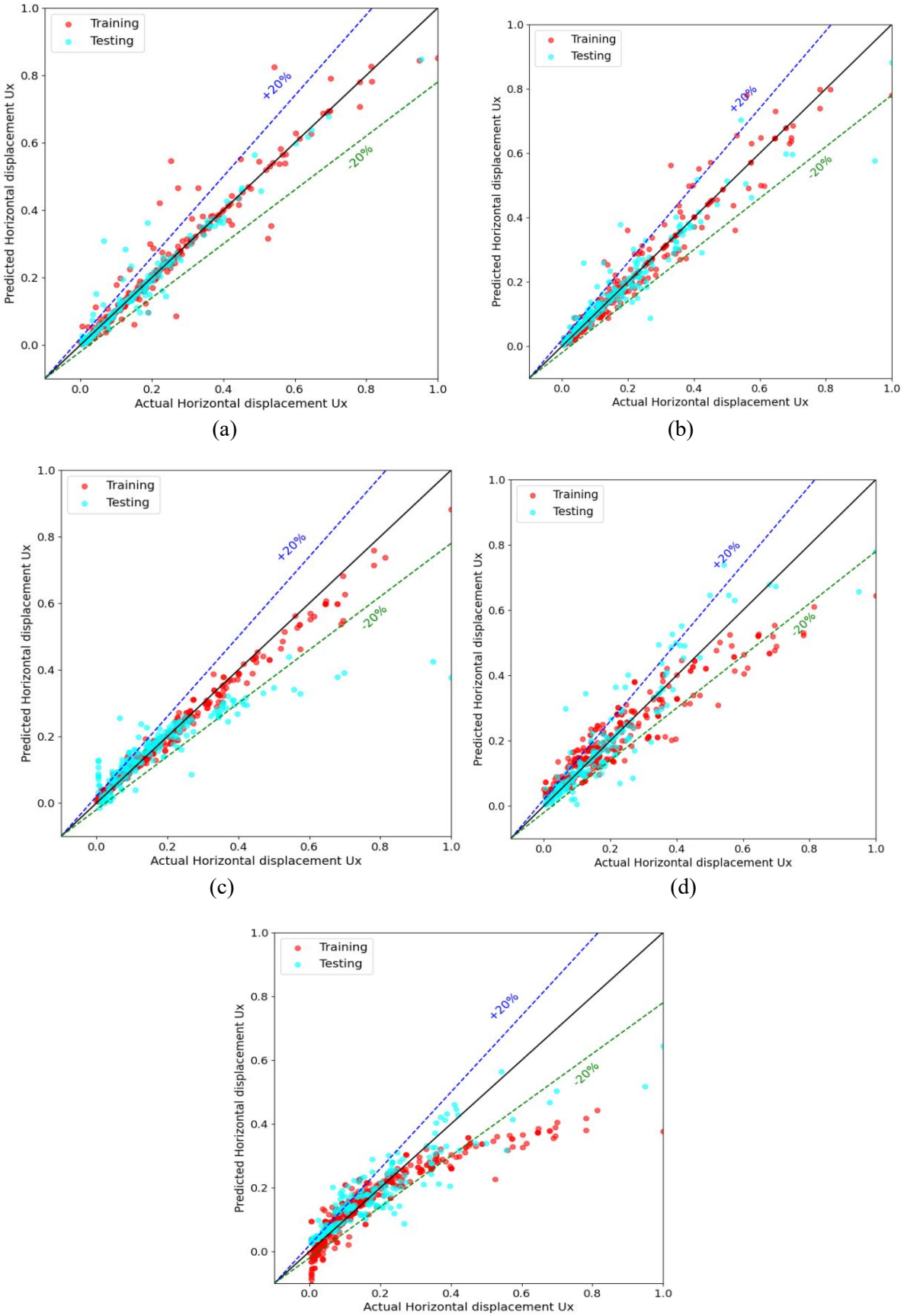

Fig. 7. Correlation between observed and predicted training and testing values for **:(a**) MLP; (**b)** RF; (**c)** KNN; (**d)** LKS; and (**e)** SVM.

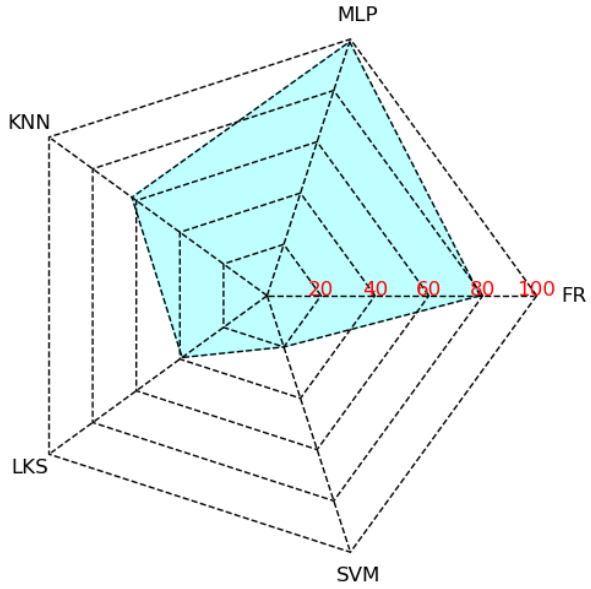

Fig. 8. Ranking of Soft Computing Models.

5.1.2. Visual interpretation

The Taylor diagram, originally proposed by Taylor (2001) [50], illustrated in Figure 9, visually compares the predictive performance of the models during both training and testing phases. These diagrams consider multiple performance metrics, including standard deviation and correlation, to assess how well the models' predictions match the actual [50]. The MLP model, represented by a dark blue dot, is positioned closest to the ideal reference point, signifying the highest predictive accuracy with a strong balance between correlation and variability. This suggests that the MLP model effectively captures the underlying data patterns and generalizes new data well. While the other models show varying levels of performance, they need to improve the MLP's accuracy. The RF and KNN models perform reasonably well but exhibit slightly more deviation and less correlation compared to the MLP. On the other hand, the LKS and SVM models demonstrate moderate to weak performance, indicating their limitations in handling the complexity of the data.

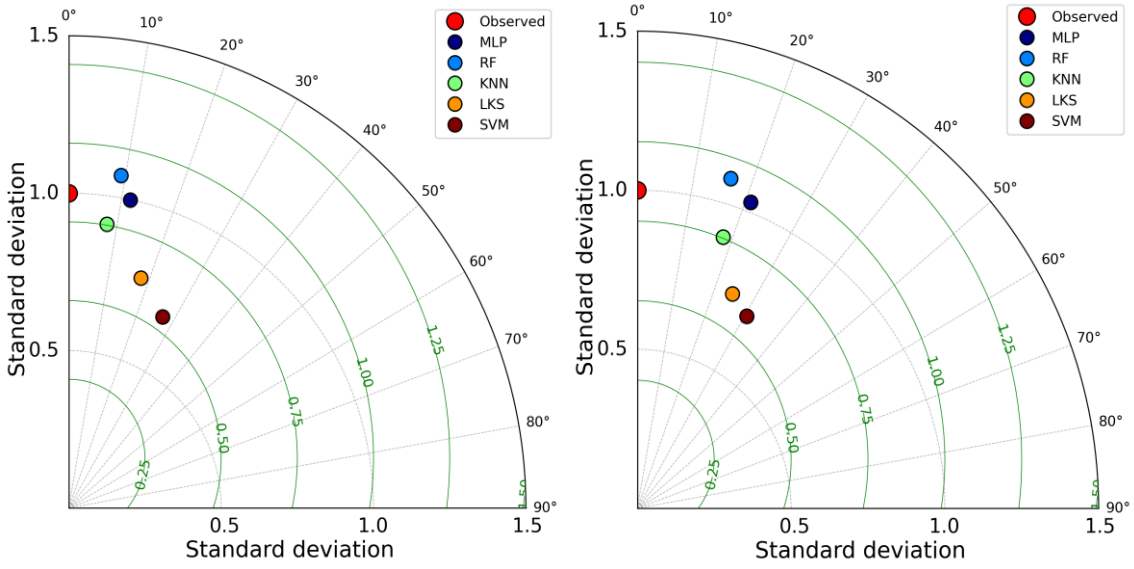

Fig. 9. Taylor diagrams for MLP, SVM, KNN, LKS and RF Models (a) training and (b) testing.

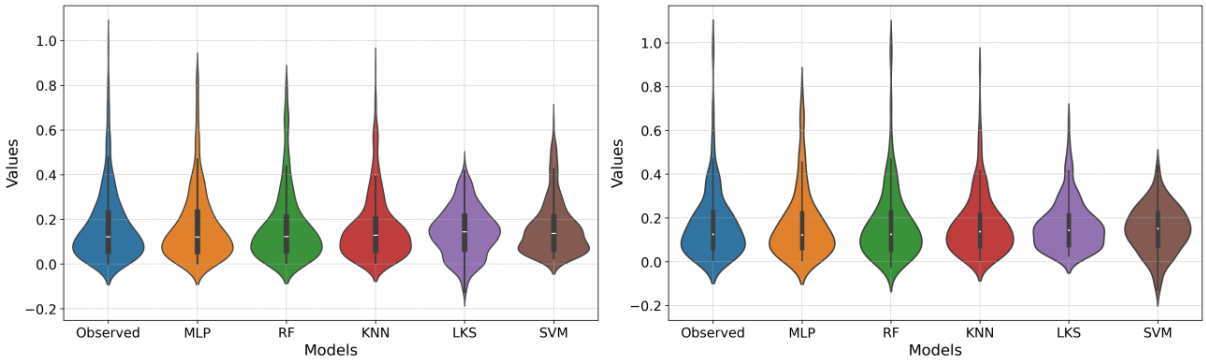

Fig. 10. Violin plots showing the probability distributions of AI model predictions compared to measured data.**(a)**Training and **(b)** Testing.

Figure 10 employs violin plots to graphically contrast the predicted data from the studied models with the observed values. These charts display the probability distribution of the predictions, offering insights into the accuracy of the models in replicating the real data during both the training and testing phases.

The violin plot of the Multilayer Perceptron (MLP) model closely resembles the distribution of the observed data, indicating a strong alignment between the model's predictions and the actual values. This similarity in shape and data distribution suggests that the MLP model effectively captures the underlying patterns within the data, resulting in accurate predictions. Although the other models exhibit different degrees of alignment, they achieve a different level of precision than the MLP. The RF model has a satisfactory level of accuracy but exhibits slightly higher levels of variability. On the other hand, the KNN model is wider in scope, suggesting less exact predictions. The LKS and SVM models demonstrate the least amount of alignment, indicating their difficulties in adequately representing the intricacy of the data.

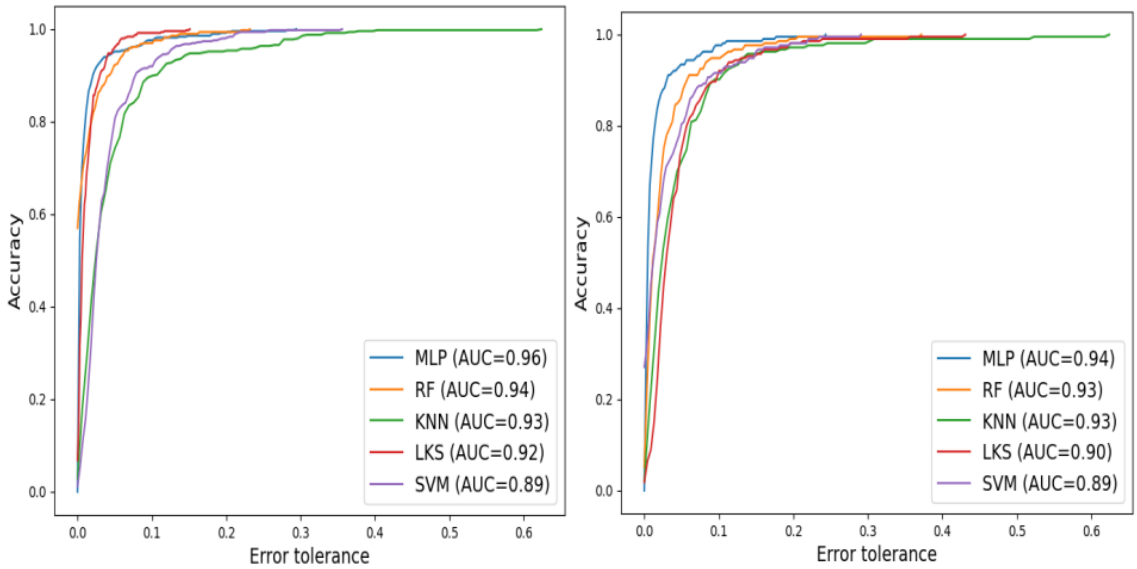

Fig. 11. illustration of REC curve for (a) Training, and (b) Testing.

Regression Error Characteristic (REC) curves, analogous to ROC curves used in classification, visually illustrate the relationship between error tolerance and the percentage of predicted points falling within a specified tolerance. The X-axis represents error tolerance, expressed as either squared error or absolute deviation, while the Y-axis shows the percentage of points within that tolerance. This curve helps estimate the cumulative distribution function of the error. The ideal model is located in the upper left corner of the

REC curve, indicating high accuracy. The closer the curve approaches this point, the more accurate the model is. Figure 11 presents the REC curves for both the training and testing phases of MLP, SVM, LKS, KNN, and RF models, illustrating the performance of each model in predicting outcomes.

The area under the curve (AUC) for both the training and testing phases of each model is calculated and visualized in Figure 11. This metric provides a comprehensive assessment of model performance, considering the balance between true positive and false positive rates. The Multi-Layer Perceptron (MLP) model exhibits the highest accuracy with an AUC of 0.96 for training and 0.94 for testing, demonstrating its superior ability to predict outcomes accurately. The Random Forest (RF) and K-Nearest Neighbors (KNN) models are closely followed, and they also demonstrate strong predictive performance. The Lazy K-Star (LKS) model performs well with an AUC of 0.93 for training and 0.90 for testing but falls slightly behind the top three models. While the Support Vector Machine (SVM) model achieves an AUC of 0.89 in both the training and testing phases, it exhibits the lowest AUC among the compared models. Despite this, the SVM model still demonstrates competent accuracy but is outperformed by the other models in this analysis.

According to the comparisons conducted in the previous section, the MLP model has demonstrated strong effectiveness in predicting the horizontal displacement of MSE walls. To further validate its performance, it is essential to explore how various input variables affect the model's predictions. To achieve this, we carried out both a sensitivity analysis and a one-factor-at-a-time (OAT) analysis. The findings from these analyses are detailed in the next section.

5.2. Model robustness and sensitivity analysis

5.2.1. One factor at a time (OAT) analysis

A sensitivity analysis was conducted to understand how individual input variables influence the model's predictions of horizontal displacement (U_x). This involved systematically varying one input variable at a time while keeping others constant, a technique known as one-factor-at-a-time (OAT) analysis [51]. Input values were chosen within the range of the original data, and twenty incremental steps were used for each variable. The model's robustness was assessed by comparing its predicted trends with established geotechnical principles governing MSE wall displacement.

Figures 12a, 12b and 12c illustrate the predicted trends of horizontal displacement (U_x) based on various factors. Figure 12a shows the influence of reinforcement characteristics, including length (L), vertical spacing (S_v), and stiffness (EA). Figure 12b depicts how embankment geometry, such as height (H), length (B), and inclination angle (α), affects U_x. Figure 12c highlights the role of embankment characteristics, specifically the friction angle (φ) and unit weight (γ).

Regarding the reinforcement characteristics, increasing vertical reinforcement spacing (S_v) leads to higher horizontal displacement (U_x). Conversely, increasing reinforcement stiffness (EA) and reinforcement length (L) results in lower U_x values. Abdelouahab (2011) [32] demonstrated this finding when modeling MSE walls using the finite difference method.

In terms of embankment geometry, an increase in wall height (h) resulted in higher horizontal displacement (U_x), while a longer embankment length (B) led to lower U_x values. Additionally, variations in the inclination angle (α) had little effect on horizontal displacement. Similar findings were reported by Gopika and Sudheesh (2021) [52]in their study of back-to-back MSE walls with trapezoidal marginal fill. For the case of embankment characteristics, an increase in unit weight (γ) resulted in a larger U_x. In comparison, an increase in the embankment's friction

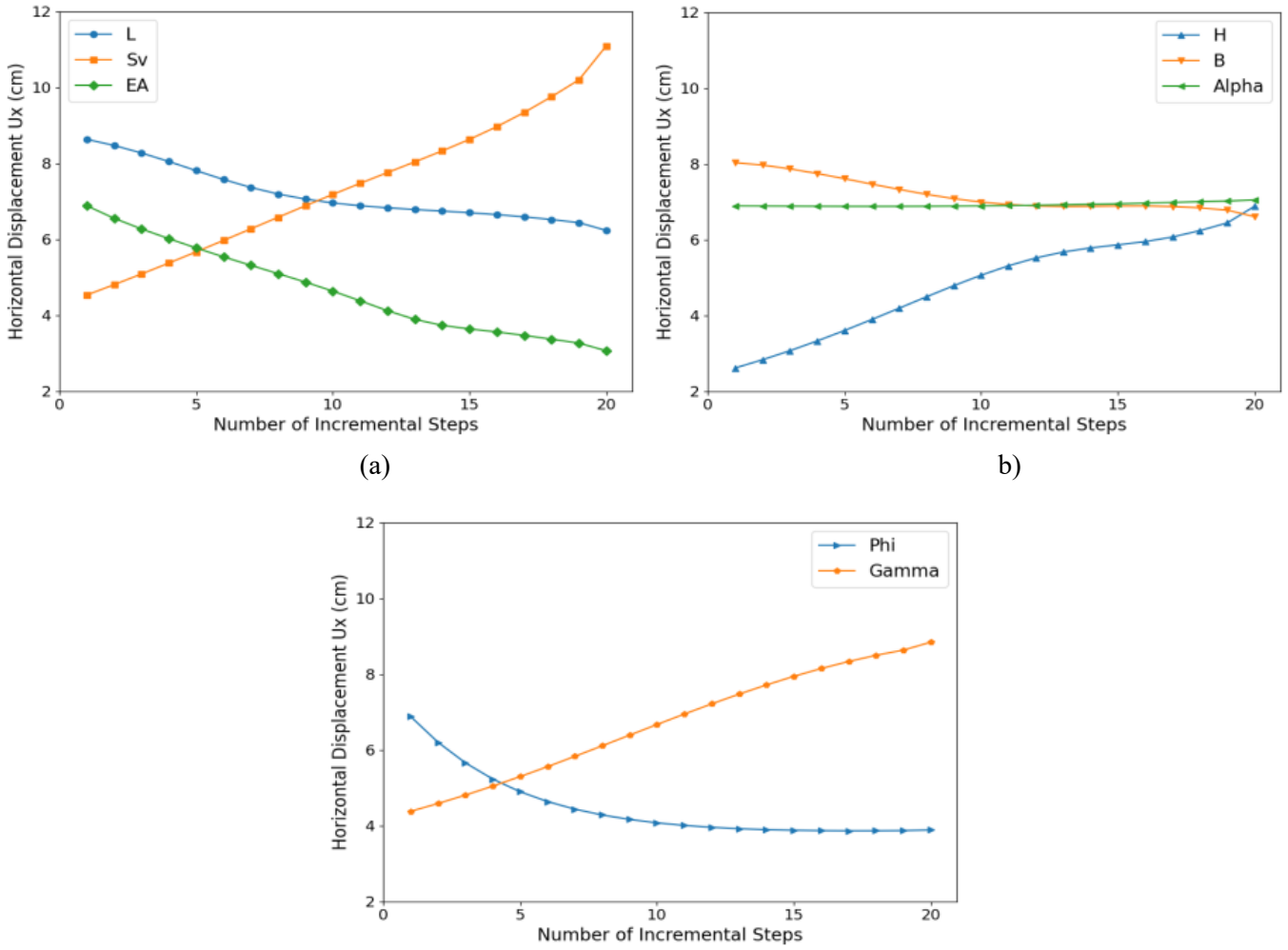

Fig. 12. One-factor-at-a-time (OAT) analysis of the developed MLP Model: (a) reinforcement characteristics, (b) embankment geometric, (c) embankment characteristics.

angle (φ) resulted in a lower U_x. Hamrouni et al. (2018) [53] found similar results when examining the reliability analysis of a mechanically stabilized earth (MSE) wall utilizing the surface response methodology.

5.3. Sensitivity analysis

Sensitivity analysis determines how each input affects a model's output. The Cosine Amplitude Method (CAM) is one such technique that identifies relationships between parameters by representing all data in a common space (X-space) [54]. This involves creating a data array (X) from paired data points.

$$X = \{x_1, x_2, x_3, \ldots, x_m\} \quad (21)$$

Each of the elements, X_i, in the data array X is a vector of lengths of m, that is:

$$x_i = \{x_{i1}, x_{i2}, x_{i3}, \ldots, x_{im}\} \quad (22)$$

Using Equation (22) [55], we can calculate the strength of the relationship, denoted as SS_{ij}, between any two data points, x_i and x_j.

$$SS_{ij} = \frac{\sum_{k=1}^{m} x_{ik} x_{jk}}{\sqrt{\sum_{k=1}^{m} x_{ik}^2 \sum_{k=1}^{m} x_{jk}^2}}, \; 0 \leq SS_{ij} \leq 1 \quad (23)$$

Figure 13 presents the results of a sensitivity analysis using the Cosine Amplitude Method (CAM) for an MLP model. The analysis investigated the influence of eight input parameters (L, S_v, H, B, α, EA, φ, and γ) on the horizontal displacement (U_x) of the model. The analysis found that the height of the wall (H) has the strongest correlation with the horizontal displacement, followed by the vertical spacing of the reinforcement (S_v), the angle of inclination (α), the length of the embankment (B), the unit weight (γ), reinforcement length (L), and friction angle (φ).

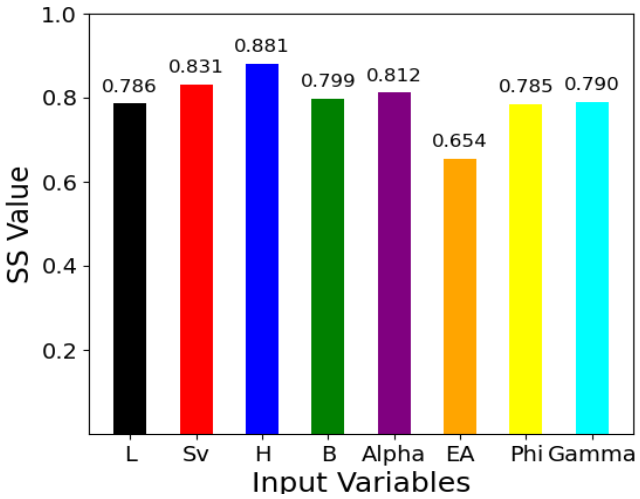

Fig .13. Strengths of relation (SS_{ij}) between input parameters and horizontal displacement for the developed MLP model.

These parameters exhibited correlations of 88.10%, 83.10%, 81.20%, 79.90%, 79.0%, 78.6%, and 78.5% respectively. In contrast, the reinforcement stiffness (EA) showed a significantly lower correlation with the horizontal displacement at 65.4%.

6. Conclusions

This research addresses the critical challenge of predicting the horizontal displacement (U_x) of Mechanically Stabilized Earth (MSE) walls, which are widely used in geotechnical engineering due to their cost-effectiveness and ease of construction. MSE walls incorporate geosynthetic materials to reinforce the soil, providing stability for various infrastructure projects, such as highway ramps and bridge-approach embankments.

The primary objective of this study was to evaluate the performance of five AI-based machine learning models in predicting the horizontal displacement of Mechanically Stabilized Earth (MSE) walls. The models investigated included Multilayer Perceptron (MLP), Support Vector Machine (SVM), k-Nearest Neighbor (KNN), Lazy k-Star (LKS), and Random Forest (RF). A dataset of 712 numerical simulations was generated using the finite element software Plaxis 2D, with each sample comprising eight input variables: reinforcement length (L), vertical spacing of reinforcement (S_v), wall height (H), length of the embankment (B), angle of inclination of the embankment (α), stiffness of reinforcement (EA), friction angle (φ), and unit weight (γ). The output variable was the horizontal displacement (U_x). The dataset was split into a 70% training set and a 30% testing set to facilitate model training and evaluation.

The performance of the models was evaluated using ten statistical metrics, including RMSE, R^2, MAE, SI, RAE, RRSE, LMI, VAF, Adj. R^2, and SMAPE. A comprehensive ranking analysis identified the Multilayer Perceptron (MLP) model as the top performer. MLP achieved the highest R^2 scores (0.9818 training, 0.9498 testing) and the lowest error rates, with MAE of 0.0124 (training) and 0.0136 (testing), and RMSE of 0.0214

(training) and 0.0319 (testing). These results underscore the MLP model's exceptional ability to capture complex data patterns, demonstrating its high accuracy and reliability in predicting horizontal displacement.

The Random Forest (RF) model performed closely behind the top performer, achieving R^2 values of 0.9588 (training) and 0.9004 (testing), with competitive error metrics: MAE of 0.0130 (training) and 0.0251 (testing). The K-Nearest Neighbors (KNN) model also showed strong performance, with R^2 values of 0.9569 (training) and 0.8618 (testing), though its MAE was slightly higher at 0.0111 (training) and 0.0306 (testing). Both models demonstrated reliable predictive accuracy, with RF slightly outperforming KNN.

In contrast, the Lazy k-Star (LKS) and Support Vector Machine (SVM) models exhibited weaker predictive capabilities. LKS achieved moderate R^2 values of 0.8710 (training) and 0.7988 (testing), but with higher error metrics: MAE of 0.0383 (training) and 0.0444 (testing). SVM performed the poorest, with R^2 values of 0.7348 (training) and 0.7067 (testing) and the highest MAE of 0.0457 (training) and 0.0438 (testing). Overall ranking scores further highlighted the MLP model's superiority with a score of 99, followed by RF (79) and KNN (62), while LKS and SVM scored significantly lower at 39 and 20, respectively. These results underscore the limited predictive performance of LKS and SVM compared to the top-performing models.

Visual interpretation tools, such as Taylor plots, REC curves, and violin plots, were used to assess the models' predictive capabilities. The Taylor diagram highlighted the MLP model's exceptional accuracy, placing it closest to the ideal reference point, indicating a strong balance between correlation and variability. Violin plots further confirmed the MLP's precision, showing a high similarity to observed values. The REC curves and their AUC metrics reinforced these results, with the MLP model achieving the highest AUC values of 0.96 (training) and 0.94 (testing), underscoring its superior performance.

The robustness of the MLP model was validated through sensitivity analysis using the Cosine Amplitude Method (CAM) and One-Factor-at-a-Time (OAT) analysis. These methods identified the vertical spacing of reinforcement (S_v) and wall height (H) as the most influential parameters affecting horizontal displacement (U_x). The MLP model consistently demonstrated reliable performance across various parameter variations, confirming its robustness and reliability in predicting U_x.

In conclusion, this research demonstrated the effectiveness of AI-based machine learning models, particularly the Multilayer Perceptron (MLP), in accurately predicting the horizontal displacement of Mechanically Stabilized Earth (MSE) walls. The study's comprehensive approach, including extensive data collection, rigorous evaluation, and sensitivity analysis, ensures reliable and applicable findings. Despite these promising results, this study has certain limitations that should be considered. The findings are dependent on the specific dataset generated using Plaxis 2D, which may not fully capture the variability and complexity of real-world MSE wall behavior. The performance of the models may be limited when applied to data outside the ranges of the dataset used.

CRediT authorship contribution statement

Saloua Hamza: Investigation; Modelling; Conceptualization; Formal analysis; Writing.

Brahim Lafifi: Investigation; Methodology; Conceptualization; Formal analysis; Writing – review & editing.

Mohamed Nemissi: Methodology; Conceptualization; Soft computing; Writing.

Abdelkrim Moussaoui: Methodology; Conceptualization; Soft computing.

Ammar Rouaiguia: Investigation; Writing – review & editing.

Funding

This research was conducted independently, without any external funding that could have biased its results.

Conflicts of interest

The authors declare no conflicts of interest regarding this manuscript.

References

[1] No NHIC. Design and Construction of Mechanically Stabilized Earth Walls and Reinforced Soil Slopes – Volume I. vol. I. 2009.

[2] Rajagopal G, Thiyyakkandi S. Numerical Evaluation of the Performance of Back-to-Back MSE Walls with Hybrid Select-Marginal Fill Zones. Transp Geotech 2020:100445. https://doi.org/10.1016/j.trgeo.2020.100445.

[3] Portelinha FHM, Bueno BS, Zornberg JG. Performance of geotextile reinforced soil wall in unsaturated poorly draining backfill soil conditions. Proc 5th … 2012;5:455–9.

[4] Muteb HH, Falah MW. Mechanically Stabilized Earth MSE Walls Applications: Review. IOP Conf Ser Earth Environ Sci 2021;856. https://doi.org/10.1088/1755-1315/856/1/012031.

[5] Chaabani W, Remadna MS, Abu-Farsakh M. Numerical Modeling of the Ultimate Bearing Capacity of Strip Footings on Reinforced Sand Layer Overlying Clay with Voids. Infrastructures 2023;8:1–20. https://doi.org/10.3390/infrastructures8010003.

[6] Christopher BR, Stulgis RP. Low Permeable Backfill Soils in Geosynthetic Reinforced Soil Walls: State-of-the-Practice in North America. Proc North Am Geo-Synthetics Conf (NAGS 2005) 2005:14–6.

[7] Hossain MS, Kibria G, Khan MS, Hossain J, Taufiq T. Effects of Backfill Soil on Excessive Movement of MSE Wall. J Perform Constr Facil 2012;26:793–802. https://doi.org/10.1061/(ASCE)CF.1943-5509.0000281.

[8] Koerner RM, Koerner GR. The importance of drainage control for geosynthetic reinforced mechanically stabilized earth walls. J Geoengin 2011;6:3–13. https://doi.org/10.6310/jog.2011.6(1).1.

[9] Abu-farsakh M, Hanandeh S, Mohammad L, Chen Q. Geotextiles and Geomembranes Performance of geosynthetic reinforced / stabilized paved roads built over soft soil under cyclic plate loads. Geotext Geomembranes 2016. https://doi.org/10.1016/j.geotexmem.2016.06.009.

[10] Lafifi B, Rouaiguia A, Soltani EA. A Novel Method for Optimizing Parameters influencing the Bearing Capacity of Geosynthetic Reinforced Sand Using RSM, ANN, and Multi-objective Genetic Algorithm. Stud Geotech Mech 2023;45:174–96. https://doi.org/10.2478/sgem-2023-0006.

[11] Blivet JC, Gourc JP, Villard P, Giraud H, Khay M, Morbois A. Design method for geosynthetic as reinforcement for embankment subjected to localized subsidence. 7th Int Conf Geosynth 2002:341–4.

[12] Shukla SK. Geosynthetics and Their Applications. Thomas Telford Publ London, UK, 430 P 2002;3:31173. https://doi.org/10.1680/gata.31173.

[13] Chen Q, Hanandeh S, Abu-Farsakh M, Mohammad L. Performance evaluation of full-scale geosynthetic reinforced flexible pavement. Geosynth Int 2018;25:26–36. https://doi.org/10.1680/jgein.17.00031.

[14] Koseki J, Shibuya S. Mitigation of Disasters by Earthquakes, Tsunamis, and Rains by Means of Geosynthetic-Reinforced Soil Retaining Walls and Embankments. Transp Infrastruct Geotechnol 2014;1:231–61. https://doi.org/10.1007/s40515-014-0009-0.

[15] Skinner GD, Rowe RK. Design and behaviour of geosynthetic-reinforced soil walls constructed on yielding foundations. Geosynth Int 2003;10:200–14. https://doi.org/10.1680/gein.2003.10.6.200.

[16] Sayed S, Dodagoudar GR, Rajagopal K. Reliability analysis of reinforced soil walls under static and seismic forces 2008. https://doi.org/10.1680/gein.2008.15.4.246.

[17] Yu Y, Bathurst RJ. Probabilistic assessment of reinforced soil wall performance using response surface method. Geosynth Int 2017;24:524–42. https://doi.org/10.1680/jgein.17.00019.

[18] Nasser Sekfali BL. Mechanically Stabilized Earth Wall Reliability Analysis Using Response Mechanically Stabilized Earth Wall Reliability Analysis Using Response Surface Methodology , ANN , ANFIS and Multi-objective Genetic Algorithm 2024. https://doi.org/10.3311/PPci.22830.

[19] Umer M, Khan A, Kumar S. Transportation Geotechnics Numerical investigation of the structural response of a conduit buried within a soil slope. Transp Geotech 2021;30:100614. https://doi.org/10.1016/j.trgeo.2021.100614.

[20] Kim MK, Cho SH, Yun IJ, Won JH. Three-dimensional responses of buried corrugated pipes and ANN-based method for predicting pipe deflections. Int J Numer Anal Methods Geomech 2012;36:1–16. https://doi.org/10.1002/nag.986.

[21] Adombi AVDP, Chesnaux R, Boucher MA. Comparing numerical modelling, traditional machine learning and theory-guided machine learning in inverse modeling of groundwater dynamics: A first study case application. J Hydrol 2022;615. https://doi.org/10.1016/j.jhydrol.2022.128600.

[22] Kaloop MR, Bardhan A, Kardani N, Samui P, Hu JW, Ramzy A. Novel application of adaptive swarm intelligence techniques coupled with adaptive network-based fuzzy inference system in predicting photovoltaic power. Renew Sustain Energy Rev 2021;148:111315. https://doi.org/10.1016/j.rser.2021.111315.

[23] Abualigah L, Alkhrabsheh M. Amended hybrid multi-verse optimizer with genetic algorithm for solving task scheduling problem in cloud computing. J Supercomput 2022. https://doi.org/10.1007/s11227-021-03915-0.

[24] Abualigah L, Alkhrabsheh M. Amended hybrid multi - verse optimizer with genetic algorithm for solving task scheduling problem in cloud computing. J Supercomput 2021. https://doi.org/10.1007/s11227-021-03915-0.

[25] Mirjalili S, Gandomi AH, Mirjalili SZ, Saremi S, Faris H, Mirjalili SM. Salp Swarm Algorithm: A bio-inspired optimizer for engineering design problems. Adv Eng Softw 2017;114:163–91. https://doi.org/10.1016/j.advengsoft.2017.07.002.

[26] Goudjil K, Arabet L. Assessment of deflection of pile implanted on slope by artificial neural network. Neural Comput Appl 2021;33:1091–101. https://doi.org/10.1007/s00521-020-04985-6.

[27] Belaabed F, Goudjil K, Arabet L, Ouamane A. Utilization of computational intelligence approaches to estimate the relative head of PK-Weir for submerged flow. Neural Comput Appl 2021;33:13001–13. https://doi.org/10.1007/s00521-021-05996-7.

[28] Lafifi B, Hamrouni A, Khoualdia T, Gheris A, Rouaiguia A. Prediction and optimization of the bearing capacity of strip footing resting on soft soil improved with stone columns using RSM, ANN, and multi-objective GA. Innov Infrastruct Solut 2024;9. https://doi.org/10.1007/s41062-024-01452-2.

[29] Goudjil K, Boukhatem G, Boulifa R, Bekkouche SR, Djihane D. Prediction and interpretation of limit pressure of clayey soils using ensemble machine learning methods and shapely additive explanations. Stud Eng Exact Sci 2024;5:e5567. https://doi.org/10.54021/seesv5n2-017.

[30] Hatami K, Bathurst RJ. Development and verification of a numerical model for the analysis of geosynthethic-reinforced soil segmental walls under working stress conditions. Can Geotech J 2005;42:1066–85. https://doi.org/10.1139/t05-040.

[31] Ali T, Haider W, Ali N, Aslam M. A Machine Learning Architecture Replacing Heavy Instrumented Laboratory Tests: In Application to the Pullout Capacity of Geosynthetic Reinforced Soils. Sensors 2022;22. https://doi.org/10.3390/s22228699.

[32] Abdelouhab A, Dias D, Freitag N. Geotextiles and Geomembranes Numerical analysis of the behaviour of mechanically stabilized earth walls reinforced with different types of strips 2011;29:116–29. https://doi.org/10.1016/j.geotexmem.2010.10.011.

[33] Flavigny E, Desrues J, Palayer B. Note technique : le sable d'Hostun « RF ». Rev Française Géotechnique 1990:67–70. https://doi.org/10.1051/geotech/1990053067.

[34] Ajibona AI, Taiwo BO, Afeni TB, Akinbinu VA. Development of Efficient Empirical Models for the Prediction of Oil Well Fracture Pressure Gradient. Daffodil Int Univ J Schience Technol 2022;17:1–9.

[35] Lawal AI, Kwon S, Young G. Prediction of the blast - induced ground vibration in tunnel blasting using ANN , moth - flame optimized ANN , and gene expression programming. Acta Geophys 2021;69:161–74. https://doi.org/10.1007/s11600-020-00532-y.

[36] Sadowski L, Wang D. Pull-off adhesion prediction of variable thick overlay to the substrate 2018. https://doi.org/10.1016/j.autcon.2017.10.001.

[37] Thai B, Tien D, Prakash I, Dholakia MB. Catena Hybrid integration of Multilayer Perceptron Neural Networks and machine learning ensembles for landslide susceptibility assessment at Himalayan area (India) using GIS. Catena 2017;149:52–63. https://doi.org/10.1016/j.catena.2016.09.007.

[38] Gao W, Alsarraf J, Moayedi H, Shahsavar A, Nguyen H. Comprehensive preference learning and feature validity for designing energy-efficient residential buildings using machine learning paradigms. Appl Soft Comput J 2019;84:105748. https://doi.org/10.1016/j.asoc.2019.105748.

[39] Moayedi H, Nguyen H, Safuan A. Novel metaheuristic classification approach in developing mathematical model - based solutions predicting failure in shallow footing. Eng Comput 2019. https://doi.org/10.1007/s00366-019-00819-9.

[40] Burr T. Pattern Recognition and Machine Learning. J Am Stat Assoc 2008;103:886–7. https://doi.org/10.1198/jasa.2008.s236.

[41] Cortes C, Vapnik V. Support-vector networks. Mach Learn 1995;20:273–97. https://doi.org/10.1007/BF00994018.

[42] Hsu C, Chang C, Lin C. A Practical Guide to Support Vector Classification 2016;1:1–16.

[43] Barakat N, Bradley AP. Neurocomputing Rule extraction from support vector machines : A review. Neurocomputing 2010;74:178–90. https://doi.org/10.1016/j.neucom.2010.02.016.

[44] Hasilci B, Mumcu TV. Parameter Estimation of BLDC Motors by SVM for UAV Propulsion Systems İnsansız Hava Aracı Tahrik Sistemleri İçin SVM ile BLDC Motorların Parametre Kestirimi 1 . Introduction UAVs , which are an important part of the rapidly developing world technologies , 2022;15:406–19. https://doi.org/10.18185/erzifbed.930222.

[45] Altman NS. An introduction to kernel and nearest-neighbor nonparametric regression. Am Stat 1992;46:175–85. https://doi.org/10.1080/00031305.1992.10475879.

[46] Ho TK. Random decision forests. Proc. Int. Conf. Doc. Anal. Recognition, ICDAR, vol. 1, 1995, p. 278–82. https://doi.org/10.1109/ICDAR.1995.598994.

[47] Breiman LEO. Random Forests 2001:5–32.

[48] Cleary JG, Trigg LE. K*: An Instance-based Learner Using an Entropic Distance Measure. Mach. Learn. Proc. 1995, vol. 5, Elsevier; 1995, p. 108–14. https://doi.org/10.1016/B978-1-55860-377-6.50022-0.

[49] Webb G. Lazy Learning. In: Sammut C, Encyclopedia of Machine Learning. 2011.

[50] Taylor KE. in a single diagram 2001;106:7183–92.

[51] Saltelli A, Annoni P, Hombres BD. Sixth International Conference on Sensitivity Analysis of Model Output How to avoid a perfunctory sensitivity analysis. Soins Aides-Soignantes 2010;2:7592–4. https://doi.org/10.1016/j.sbspro.2010.05.133.

[52] Rajagopal G, Thiyyakkandi S. Influence of Retained Zone Width on the Behaviour of Back - to - Back Mechanically Stabilized Earth Walls upon Rainwater Infiltration. Int J Geosynth Gr Eng 2022;8:1–14. https://doi.org/10.1007/s40891-022-00416-9.

[53] Hamrouni A, Dias D, Sbartai B. Reliability analysis of a mechanically stabilized earth wall using the surface response methodology optimized by a genetic algorithm. Geomech Eng 2018;15:937–45. https://doi.org/10.12989/gae.2018.15.4.937.

[54] Rezaei M, Asadizadeh M, Majdi A, Hossaini MF. International Journal of Mining Science and Technology Prediction of representative deformation modulus of longwall panel roof rock strata using Mamdani fuzzy system. Int J Min Sci Technol 2015;25:23–30. https://doi.org/10.1016/j.ijmst.2014.11.007.

[55] Ghorbani B, Arulrajah A, Narsilio G, Horpibulsuk S, Bo MW. Development of genetic-based models for predicting the resilient modulus of cohesive pavement subgrade soils. Soils Found 2020;60:398–412. https://doi.org/10.1016/j.sandf.2020.02.010.